Organic Geochemistry 150 (2020) 104128

Contents lists available at ScienceDirect

Organic Geochemistry

journal homepage: www.elsevier.com/locate/orggeochem

Effects of Mississippi valley-type minerogenetic metal sulfates on thermochemical sulfate reduction, studied by hydrous pyrolysis

Jing Liao [a], Taoli Wang [a,b], Hong Lu [a,*], Paul F. Greenwood [c,d], Ping'an Peng [a], Chang Samuel Hsu [e,f,g]

[a] State Key Laboratory of Organic Geochemistry, Guangzhou Institute of Geochemistry, Institutions of Earth Science, Chinese Academic of Sciences, Guangzhou 510640, China
[b] University of Chinese Academic of Sciences, Beijing 100049, China
[c] School of Earth Sciences, University of Western Australia, Crawley, WA 6009, Australia
[d] Western Australia Organic and Isotope Geochemistry Centre, School of Earth and Planetary Sciences, Curtin University, GPO Box U1987, Perth, WA 6845, Australia
[e] Petro Bio Oil Consulting, Tallahassee, FL 32312, United States
[f] Department of Chemical and Biomedical Engineering, Florida A & M University/Florida State University, Tallahassee, FL 32310, United States
[g] State Key Laboratory of Heavy Oil Processing, China University of Petroleum, Beijing 102249, China

ARTICLE INFO

Article history:
Received 27 April 2020
Received in revised form 13 September 2020
Accepted 16 September 2020
Available online 24 September 2020

Keywords:
TSR
Hydrous pyrolysis experiment
MVT
Sulfates
$FeSO_4$
N-octadecane
Pyrite

ABSTRACT

Mississippi valley-type (MVT) ore deposits are epigenetic carbonate-hosted Pb-Zn deposits, that are formed by fluid expulsion from sedimentary sulfide successions. The sulfides were generated by thermochemical sulfate reduction (TSR) of the evaporitic sulfates dissolved in fluids. The initiation, processes and principles for TSR occurring in MVT ore deposition and the respective influence of major minerogenetic metal ions such as Pb^{2+} and Zn^{2+}, as well as Fe^{2+}, Sr^{2+}, Ba^{2+} has not been clearly resolved. To evaluate the TSR activity of metal cations in MVT minerogenetic systems, a series of 300 °C to 450 °C gold-tube hydrous-pyrolysis experiments were separately conducted with $FeSO_4$, $PbSO_4$, $ZnSO_4$, $BaSO_4$ or $SrSO_4$ and with *n*-octadecane (*n*-C_{18}) as the hydrocarbon substrate. Based on the yields (from gas chromatography (GC) analysis) and carbon isotopic compositions (determined by GC-irMS) of the gases produced in the hydrous-pyrolysis gold-tube experiments, the TSR reactivity of the minerogenetic metal sulfates was ranked $FeSO_4$ > $ZnSO_4$ > Sr/$BaSO_4$ > $PbSO_4$. TSR occurred easily in the $FeSO_4$ experiments at 300 °C, but hardly at all in $PbSO_4$ experiments at 450 °C. Hence, S^{2-} for the formation of the gelenite (PbS), sphalerite (ZnS) and pyrite (FeS_2) in the MVT ore deposits appears to be related to Fe^{2+}, which could initiate the TSR easily to produce reduced sulfur.

The following two potential routes would provide good support for the TSR of $FeSO_4$: (1) Hydrolysis of Fe^{2+}, or the formation of a ferrous hydroxide-sulfate-hydrate complex, that increases the H^+ concentration, resulting in the formation of HSO_4^- that initiates TSR; and (2) The oxidation of Fe^{2+} to Fe^{3+}, which on subsequent hydrolysis (or the formation of iron-hydroxide-sulfate-hydrate complex), would greatly increase the concentrations of H^+ and HSO_4^-, reduce the *pH* of the brine fluids and maintain acidic conditions favorable to TSR. However, the precipitation of pyrite greatly consumes S^{2-}, limiting the concentration of H_2S and thereby affecting the rate of TSR.

In short, TSR is difficult to simulate using Zn^{2+} and Pb^{2+} sulfates, but easy with sulfates containing Fe^{2+} and Mg^{2+}. This suggests that the occurrence of the $FeSO_4$ and $MgSO_4$ is critical in the formation of the large-scale MVT ore deposits, where they react as acid buffering agents, decreasing and maintaining a lower *pH* in the brine fluids and accelerating and sustaining TSR with higher concentrations of HSO_4^-. H_2S/S^{2-} would then be produced continually and participate as FeS_2, ZnS and PbS in the large-scale MVT ore deposits.

1. Introduction

Thermochemical sulfate reduction (TSR) is a complex abiotic redox process, often simplistically referred to as the reactions of mineral metal sulfates and organic compounds (e.g., petroleum hydrocarbons) to produce H_2S and CO_2 (Worden et al., 2000; Machel, 2001; Seewald, 2003). High concentrations of H_2S (sour

* Corresponding author at: State Key Laboratory of Organic Geochemistry, Guangzhou Institute of Geochemistry and Institutions of Earth Science, Chinese Academy of Sciences, 511 Kehua Street, Tianhe District, Guangzhou 510640, China.
E-mail address: luhong@gig.ac.cn (H. Lu).

https://doi.org/10.1016/j.orggeochem.2020.104128
0146-6380/

gas) in oil reservoirs are typically attributed to TSR (Orr, 1977). In laboratory simulations, direct reduction of alkali metal sulfates (i.e., K_2SO_4 and Na_2SO_4) by hydrocarbons, does not occur much below 800 °C (Goldstein and Aizenshtat, 1994) due to the high activation energy required for the initiation of TSR (Toland, 1960; Kiyosu and Krouse, 1990; Goldstein and Aizenshtat, 1994; Cross et al., 2004). Conversely, TSR of alkaline earth metal sulfates, such as $CaSO_4$ and $MgSO_4$, occurs at relatively low temperatures (>300 °C) (Machel, 2001; Zhang et al., 2008b; Lu et al., 2010, 2011, 2012). The TSR of $MgSO_4$ proceeds rapidly in the presence of water as the aqueous magnesium-hydroxide-sulfate-hydrate complex (MHSH) produces a bisulfate (HSO_4^-) ion intermediate (Janecky and Seyfried, 1983; Tang et al., 2005; Zhang et al., 2007, 2008a; Ma et al., 2008; Lu et al., 2011; Zhang et al., 2012; He et al., 2014).

Other than for $MgSO_4$, experimental investigations of the TSR behavior of prevalent transition metal sulfates ($ZnSO_4$, $FeSO_4$) and alkaline earth metal sulfates ($SrSO_4$, $BaSO_4$) have seldom been conducted. These sulfates, plus the $PbSO_4$, are the main minerogenetic metal sulfates in brine fluids of Mississippi valley-type (MVT) ore deposits and are the focus of the present study. MVT ore deposits are epigenetic carbonate-hosted Pb-Zn deposits that commonly consist of some combinations of lead, zinc and iron sulfides (sphalerite, galena, pyrite and marcasite) accompanied by barite, celestite, fluorite, dolomite and calcite (Gregg and Shelton, 2012). They are thought to form by fluid expulsion from sedimentary successions (White, 1968; Sverjensky, 1986), a conclusion supported by most of the subsequent studies on MVT ore deposits (e.g., Nakai et al., 1990; Kesler et al., 1995; Leach et al., 2001; Abidi et al., 2010; Gregg and Shelton, 2012). The reduced sulfur was generated by TSR with evaporitic sulfates dissolved in fluids as the likely source of the sulfate (Barton, 1967; Anderson, 1975, 2008; Powell and Macqueen, 1984; Anderson and Thom, 2008; Basuki et al., 2008; Thom and Anderson, 2008; Navarro-Ciurana et al., 2017; Sośnicka and Lüders, 2019). This conclusion is substantiated by sulfur isotopic studies such as those conducted on the San Vicente MVT ore deposit (Gorzawski et al., 1990; Spangenberg et al., 1999) and Bongara area MVT ore deposit (Basuki et al., 2008). Other major MVT deposits reflecting TSR behavior include the Pine Point, Nanisivik, Cadjebut, Polaris and Mascot-Jefferson City deposits (Basuki et al., 2008). Nevertheless, the initiation process and/or the principles of the TSR for the formation of the MVT are still ambiguous, especially for the TSR reactivity of major minerogenetic metal ions (Pb^{2+}, Zn^{2+}, Fe^{2+}) and the effects of the minerogenetic metal ions on the initiation and rate of TSR.

In this study, the TSR activity and the roles of MVT minerogenetic metal ions of Pb^{2+}, Zn^{2+}, Fe^{2+}, Sr^{2+}, and Ba^{2+} were systematically evaluated by gold-tube pyrolysis experiments with *n*-octadecane separately combined with $PbSO_4{\cdot}H_2O$, $FeSO_4{\cdot}7H_2O$, $ZnSO_4{\cdot}H_2O$, $SrSO_4$, and $BaSO_4$. Through the analysis of the evolved products, we propose several mechanisms by which these metal ions can initiate and influence the rate of TSR and speculate on their significance in MVT ore deposition.

2. Materials and methods

2.1. Hydrous pyrolysis

N-octadecane (*n*-C_{18}, ≥99.0%, $\delta^{13}C = -25.3‰$) was separately reacted with hydrous ferrous sulfate ($FeSO_4{\cdot}7H_2O$, 99.95%), hydrous zinc sulfate ($ZnSO_4{\cdot}H_2O$, 99.95%), hydrous lead sulfate ($PbSO_4{\cdot}H_2O$, 99.95%), strontium sulfate ($SrSO_4$, 99.95%) and barium sulfate ($BaSO_4$, 99.95%). All experiments used a 1:3 mol/mol ratio of *n*-C_{18} to metal sulfate. Water was also added to be twenty times molar mass of the sulfates (including consideration of crystal water content of sulfates). Control experiments with only *n*-C_{18} and water were conducted for comparison. The reactants were loaded into gold tubes (~60 mm length, 4.5 mm external diameter, 0.25 mm wall thickness) thermally pre-cleaned at 800 °C. The tubes were removed of air and welded closed under argon flow. Sealed gold tubes were individually placed into one of 12 autoclaves within a furnace. The pyrolysis experiments were conducted under isothermal conditions at 300 °C, 350 °C, 400 °C and 450 °C, respectively, for 72 h at a constant pressure of 50 MPa. The tubes were weighed before and after the pyrolysis experiments to confirm the integrity of the pyrolyzed tubes (i.e., no tube breakage or product loss). A more detailed account of the pyrolysis procedure has been described by Wang et al. (2014).

To investigate the effect of water on these experiments, the same series of pyrolysis experiments (300–450 °C) were conducted with *n*-C_{18} and $FeSO_4{\cdot}7H_2O$ (1:3, mol/mol) in the absence of added water. $FeSO_4$ was used for this investigation since it was proven to be the most reactive metal-sulfate used in our study.

2.2. Gaseous product analysis

The organic (C_1–C_5 hydrocarbons) and inorganic (CO_2, H_2 and H_2S) gaseous range products were analyzed with an auxiliary inlet coupled to a two-channel Hewlett-Packard 6890 gas chromatograph, custom (Wassen ECE) configured with eight columns (two capillary and six packed) and three detectors (one flame ionisation (FID) and two thermal conductivity (TCD) detectors (Wang et al., 2014)). Helium (for inorganic gas analysis) and nitrogen (for organic gas analysis) carrier gases were used. The chromatograph oven temperature was programmed from 70 °C (held for 5 min) to 130 °C at a rate of 15 °C/min, and then to a final temperature of 180 °C (held for 4 min) at a rate of 25 °C/min.

2.3. Bitumen analysis

Following the gas analyses, *n*-hexane was added to the gold tubes to extract higher molecular weight hydrocarbons (i.e., the bitumen fraction). The extracts were subsequently analyzed using a Trace Ultra gas chromatograph coupled to Thermo DSQ-II mass spectrometer. The chromatograph used nitrogen carrier gas at a constant flow of 1.2 mL/min with a HP-5 column (30 m × 0.32 mm i.d. × 0.25 μm film thickness). The oven temperature was programmed from 40 °C (held for 2 min) to 295 °C (held for 20 min) at a rate of 3 °C/min. 70 eV electron ionization (EI) mass spectra were acquired over a mass range of *m*/*z* 50–600.

2.4. Solid residue analysis

The residual solids following solvent extraction were analyzed using an Olympus BTX Ⅱ X-ray powder diffractometer equipped with an iron oxide light filter and a Cu K-alpha radiator (λ = 0.179 nm). Stepwise scanning measurements were performed at a rate of 2 °C/min in the range of 3° to 85° (2θ). Mineral abundances (%) were semi-quantitatively determined from respective peak areas with correction for Lorentz Polarization.

3. Results and discussion

3.1. Gas yields and carbon isotopic compositions

The yields of organic (C_1–C_5) and inorganic (CO_2) gases produced by the pyrolysis experiments are shown in Fig. 1 and Table 1. The H_2 and H_2S yields of some experiments are also listed in Table 1.

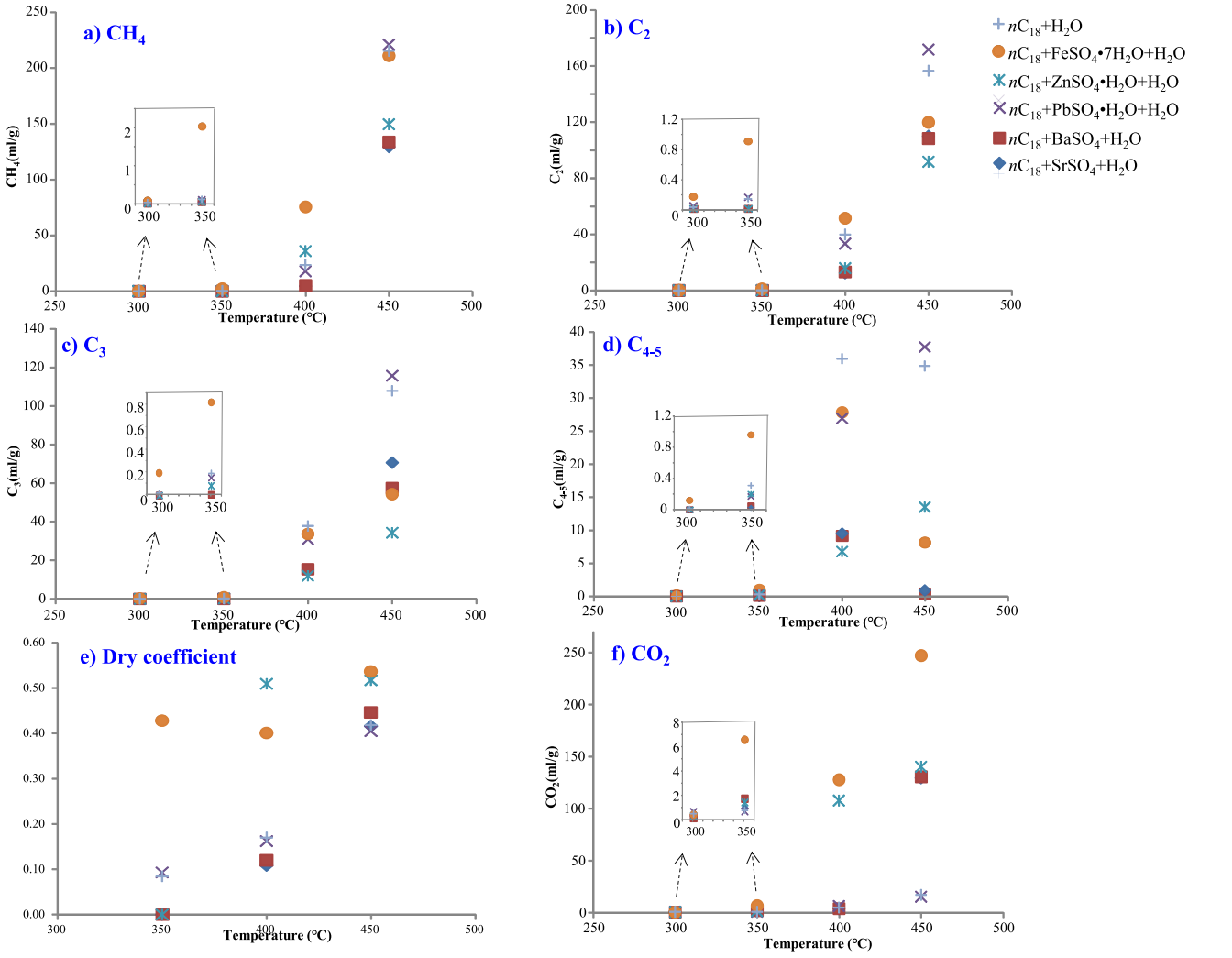

Fig. 1. The gas yields of C_1-C_5 and CO_2 from organic *n*-C_{18} and inorganic reactants $FeSO_4{\cdot}7H_2O$, $ZnSO_4{\cdot}H_2O$, $SrSO_4$, $BaSO_4$ and $PbSO_4{\cdot}H_2O$ pyrolysis experiments and the blank experiment of *n*-C_{18} and water at 300 °C, 350 °C, 400 °C, 450 °C, respectively, for 72 h.

3.1.1. Gas yields of CO_2, H_2 and H_2S

In the control experiments without any sulfate minerals, where no TSR could occur, no H_2S was produced. Only CO_2 was produced from redox reactions of hydrocarbons with water (Fig. 1, Table 1). For pyrolysis ≤ 350 °C the CO_2 yields were very low (<0.9 mL/g), increasing to 4.78 mL/g at 400 °C. The yields of H_2 were below the detection limit, indicating weak redox reactions. At 450 °C, the yield of CO_2 increased to 17.01 mL/g with a low yield of H_2 (0.01 mL/g), indicating an increase in redox rate.

At 350 °C in the metal sulfate series (Fig. 1, Table 1), the yield of CO_2 in the $FeSO_4$ pyrolysis experiments was significantly greater than the 350 °C control experiment. No H_2 was detected, indicating that the increased CO_2 was not from the hydrocarbon oxidation by water, but rather from the hydrocarbon oxidation of TSR. The low amounts of CO_2 produced with the other metal sulfates were similar to control levels, showing no occurrence of TSR. At 400 °C, the $FeSO_4$ experiment showed the highest CO_2 yield. At this pyrolysis temperature, the CO_2 yield of the $ZnSO_4$ experiment was also substantially greater than the control experiment, while the CO_2 yield of the other metal sulfates still showed little difference to the control levels. We conclude that at 400 °C TSR only occurred in the $FeSO_4$ and $ZnSO_4$ experiments. At 450 °C, CO_2 levels were 15x control with $FeSO_4$ and ~8x control with each of $ZnSO_4$, $SrSO_4$ and $BaSO_4$, indicating that TSR occurred in the $FeSO_4$, $ZnSO_4$, $SrSO_4$ and $BaSO_4$ experiments. The CO_2 yield in the $PbSO_4$ experiment was close to that of the control experiments at 300 °C, 350 °C, 400 °C and 450 °C, indicating that no TSR occurred over the full pyrolysis range investigated.

The production of H_2S provided additional evidence of TSR. H_2S (0.25 mL/g, Table 1) was detected in the $FeSO_4$ experiment at 300 °C, showing that the TSR initiating temperature in the $FeSO_4$ experiment was as low as 300 °C or even lower. The H_2S yield increased with increasing temperature and reached a maximum at, or around, 400 °C (67.2 mL/g) and then decreased to zero at 450 °C. The variation in H_2S yields with temperatures is similar to that in the $MgSO_4$ pyrolysis experiment conducted by Zhang et al. (2008b). In the $MgSO_4$ pyrolysis experiments, the H_2S yield began to decrease at the temperature where sulfur species and aromatic compounds increased (Zhang et al. 2008b). The decrease in H_2S yield might not indicate the weakening of TSR, since most of the H_2S had converted into organic sulfur compounds and element sulfur. Indeed, the production and accumulation of dibenzothiophene and elemental sulfur was observed in the $FeSO_4$ experiments at pyrolysis temperatures ≥ 400 °C (Fig. 3e, 3f). Similar phenomena have been also observed in natural systems. For example, organic sulfur biomarkers detected in high-sulfur crude oils in the Jinxian depression in China have been attributed to the reaction of H_2S with hydrocarbons (Lu et al., 2013).

Table 1
Gas yields (mL/g-*n*-C_{18}) of hydrous pyrolysis experiments.

Temperature (°C)	*n*-C_{18}	Sulfates	H_2O	Time (D)	C_1 (ml/g)	C_2 (ml/g)	C_3 (ml/g)	C_{4-5} (ml/g)	Dry coefficient ($C_1/\Sigma(C_1$-$C_5)$)	CO_2 (ml/g)	H_2 (ml/g)	H_2S (ml/g)
300	+		+	3	0.02	0.02	0.02	0.01	0.29	0.62	0	0
300	+	$PbSO_4{\cdot}H_2O$	+	3	0.02	0.04	0.00	0.00	0.33	0.77	0	n/a
300	+	$FeSO_4{\cdot}7H_2O$	+	3	0.07	0.16	0.20	0.12	0.13	0.55	0	0.25
300	+	$FeSO_4{\cdot}7H_2O$		3	0.01	0.03	0.03	0.04	0.09	0.62	0	0.04
300	+	$ZnSO_4{\cdot}H_2O$	+	3	0.00	0.00	0.00	0.00	0.00	0.44	0	n/a
300	+	$SrSO_4$	+	3	0.00	0.00	0.00	0.00	0.00	0.43	0	n/a
300	+	$BaSO_4$	+	3	0.00	0.00	0.00	0.00	0.00	0.27	0	n/a
350	+		+	3	0.06	0.13	0.20	0.01	0.08	0.89	0	0
350	+	$PbSO_4{\cdot}H_2O$	+	3	0.05	0.15	0.16	0.18	0.09	0.81	0	n/a
350	+	$FeSO_4{\cdot}7H_2O$	+	3	2.07	0.97	0.83	0.97	0.43	6.69	0	1.30
350	+	$FeSO_4{\cdot}7H_2O$		3	1.07	0.75	0.71	0.88	0.31	3.24	0	1.04
350	+	$FeSO_4{\cdot}7H_2O$		15	20.5	11.4	9.7	11.3	0.39	48.8	0	0
350	+	$ZnSO_4{\cdot}H_2O$	+	3	0.00	0.00	0.09	0.21	0.00	1.54	0	n/a
350	+	$SrSO_4$	+	3	0.00	0.00	0.01	0.04	0.00	1.06	0	n/a
350	+	$BaSO_4$	+	3	0.00	0.00	0.01	0.06	0.00	1.86	0	n/a
400	+		+	3	23.25	39.88	37.77	35.95	0.17	4.78	0	0
400	+	$PbSO_4{\cdot}H_2O$	+	3	17.65	33.32	30.93	26.93	0.16	6.33	0	n/a
400	+	$FeSO_4{\cdot}7H_2O$	+	3	75.48	51.51	33.59	27.84	0.40	127.73	0	67.23
400	+	$FeSO_4{\cdot}7H_2O$		3	53.89	42.02	26.19	19.39	0.38	100.99	0	54.48
400	+	$ZnSO_4{\cdot}H_2O$	+	3	35.85	15.83	11.97	6.77	0.51	107.72	0.01	n/a
400	+	$SrSO_4$	+	3	4.46	12.49	14.85	9.53	0.11	3.59	0.04	n/a
400	+	$BaSO_4$	+	3	5.10	13.16	15.27	9.14	0.12	3.72	0.03	n/a
450	+		+	3	215.12	156.59	107.75	34.86	0.42	17.01	0.01	0
450	+	$PbSO_4{\cdot}H_2O$	+	3	220.77	171.72	115.62	37.74	0.40	15.33	0	n/a
450	+	$FeSO_4{\cdot}7H_2O$	+	3	210.90	119.77	54.29	8.14	0.54	247.01	0.01	0
450	+	$FeSO_4{\cdot}7H_2O$		3	159.83	92.04	43.17	6.83	0.53	148.16	0	0
450	+	$FeSO_4{\cdot}7H_2O$		15	93.0	0.4	0.04	0.02	0.995	443.6	1.5	0
450	+	$ZnSO_4{\cdot}H_2O$	+	3	149.47	91.81	34.24	13.50	0.52	140.03	0.05	n/a
450	+	$SrSO_4$	+	3	129.28	110.12	70.58	0.89	0.42	129.47	0	n/a
450	+	$BaSO_4$	+	3	133.68	108.37	57.38	0.39	0.45	130.40	0	n/a

Table 2
Carbon isotopic compositions of gas yields (C_1-C_3 and CO_2) produced in the hydrous pyrolysis experiments.

Temperature(°C)	*n*-C_{18}	Sulfates	H_2O	Time (D)	C_1 (‰)	C_2 (‰)	C_3 (‰)	CO_2 (‰)
300	+		+	3		–	–	–
300	+	$PbSO_4{\cdot}H_2O$	+	3	–	–	–	–
300	+	$FeSO_4{\cdot}7H_2O$	+	3	–	–	–	–
300	+	$FeSO_4{\cdot}7H_2O$		3	–	–	–	–
300	+	$ZnSO_4{\cdot}H_2O$	+	3	–	–	–	–
300	+	$SrSO_4$	+	3	–	–	–	–
300	+	$BaSO_4$	+	3	–	–	–	–
350	+		+	3	−69.6	−43.3	−36.8	−32.1
350	+	$PbSO_4{\cdot}H_2O$	+	3	−74.5	−44.4	−36.0	−30.5
350	+	$FeSO_4{\cdot}7H_2O$	+	3	−34.9	−35.9	−32.9	−30.7
350	+	$FeSO_4{\cdot}7H_2O$		3	−37.5	−38.3	−34.2	−31.4
350	+	$FeSO_4{\cdot}7H_2O$		15	−34.9	−32.1	–	−27.0
350	+	$ZnSO_4{\cdot}H_2O$	+	3	−44.7	−40.0	−36.2	−30.2
350	+	$SrSO_4$	+	3	–	−40.6	−36.3	−27.3
350	+	$BaSO_4$	+	3	–	–	–	−28.4
400	+		+	3	−56.7	−38.8	−32.1	−33.5
400	+	$PbSO_4{\cdot}H_2O$	+	3	−55.5	−38.8	−32.1	−32.8
400	+	$FeSO_4{\cdot}7H_2O$	+	3	−38.5	−34.7	−29.2	−30.1
400	+	$FeSO_4{\cdot}7H_2O$		3	−41.0	−35.0	−28.7	−32.1
400	+	$ZnSO_4{\cdot}H_2O$	+	3	−35.6	−31.5	−28.5	−29.3
400	+	$SrSO_4$	+	3	−58.9	−40.9	−33.0	−28.3
400	+	$BaSO_4$	+	3	−55.5	−40.0	−31.9	−31.5
450	+		+	3	−41.3	−27.6	−20.9	−23.8
450	+	$PbSO_4{\cdot}H_2O$	+	3	−41.9	−28.4	−21.8	−27.1
450	+	$FeSO_4{\cdot}7H_2O$	+	3	−39.5	−27.9	−20.5	−30.3
450	+	$FeSO_4{\cdot}7H_2O$		3	−37.8	−28.9	−17.6	−31.2
450	+	$FeSO_4{\cdot}7H_2O$		15	−24.4	–	–	−26.6
450	+	$ZnSO_4{\cdot}H_2O$	+	3	−37.9	−28.3	−23.5	−28.5
450	+	$SrSO_4$	+	3	−45.7	−29.3	−23.6	−25.8
450	+	$BaSO_4$	+	3	−47.7	−30.3	−24.2	−31.0

3.1.2. Gas yields of C_1–C_5 hydrocarbons

C_1–C_5 hydrocarbons were the main gaseous products in all the pyrolysis experiments. The amount of C_1–C_3 increased substantially as temperature increased. In the controls (Fig. 1, Table 1), the C_1–C_3 yields were very low at $\leq$ 350 °C, but increased at higher temperatures to substantial levels at 450 °C. The C_{4-5} gas yields increased from 300 to 400 °C, but then showed a reduction at 450 °C. It could be rationalized that from 400 to 450 °C, C_{4-5} could

also be pyrolyzed to C_1–C_3. At low pyrolysis temperatures (≤350 °C) the C_1–C_5 yields in the $FeSO_4$ series were consistently higher than controls levels and each of the other metal sulfate series (≤350 °C). This reflects the low temperature initiation of TSR in the $FeSO_4$ experiments. At 400 °C, where hydrocarbon pyrolysis occurred extensively, the CH_4 yield of the $FeSO_4$ experiment (highest of the metal sulfates) was three times the 400 °C of the control values, yet the C_2 yields were only slightly higher and the C_3 yield was a little smaller than the corresponding control levels. At 450 °C, the yields of C_1–C_5 using all metal sulfates (except $PbSO_4$) were less than the control levels, though their CO_2 yields were greater, suggesting that the hydrocarbons in these metal sulfate experiments were oxidized to CO_2. The gas product yields in the $PbSO_4$ experiment were similar to control levels for all pyrolysis temperatures, indicating negligible impact of this metal sulfate on pyrolysis and oxidation of hydrocarbons.

3.1.3. Carbon isotopic compositions of C_1–C_3 and CO_2

The stable carbon isotopic compositions ($\delta^{13}C$) of gaseous products from all the 300 °C experiments and some experiments at 350 °C, could not be measured, due to their very low yields (Fig. 1, Table. 1). The $\delta^{13}C$ values of C_1–C_3 in the control series became heavier with increasing temperature (Fig. 2, Table 2). The lightest value (−69.6‰ at 350 °C) and the heaviest value (−41.3‰ at 450 °C) span about 30‰. This phenomenon is in accordance with classical isotope kinetics (Galimov, 2006) that light hydrocarbons pyrolyze faster than the heavier ones, contributing to the ^{12}C enrichment in the first gaseous products (C_1–C_3) at low temperature (350 °C). Thus, the $\delta^{13}C$ values of the C_1–C_3 would become heavier as the pyrolysis temperature increased. The results in the majority of metal sulfate experiments showed the same general trends in $\delta^{13}C$; however, CH_4 in the $FeSO_4$ series from 350 °C to 450 °C and the $ZnSO_4$ series from 400 °C to 450 °C showed no changes with increasing temperatures (Fig. 2, Table 2). At the same time, their $\delta^{13}C$ values were heavier than that of CH_4 produced in the control series, indicated that these CH_4 were altered by TSR. In the non-isothermal simulation experiments, light hydrocarbon gases reacted preferentially during TSR, resulting in increase in the $\delta^{13}C$ of residual hydrocarbon gases (Krouse et al., 1988; Connan et al., 1995). Different trends in $\delta^{13}C$ of methane in the $FeSO_4$ (350–450 °C) and the $ZnSO_4$ series (400–450 °C) are proposed to result from kinetic isotopic fractionation of light methane ($^{12}CH_4$) which was slightly oxidized at 350 °C and 400 °C during the TSR reaction. However, previous TSR experimental simulation experiments showed that CH_4 is the least reactive of all possible reactive organic compounds due to its most stable chemical struc-

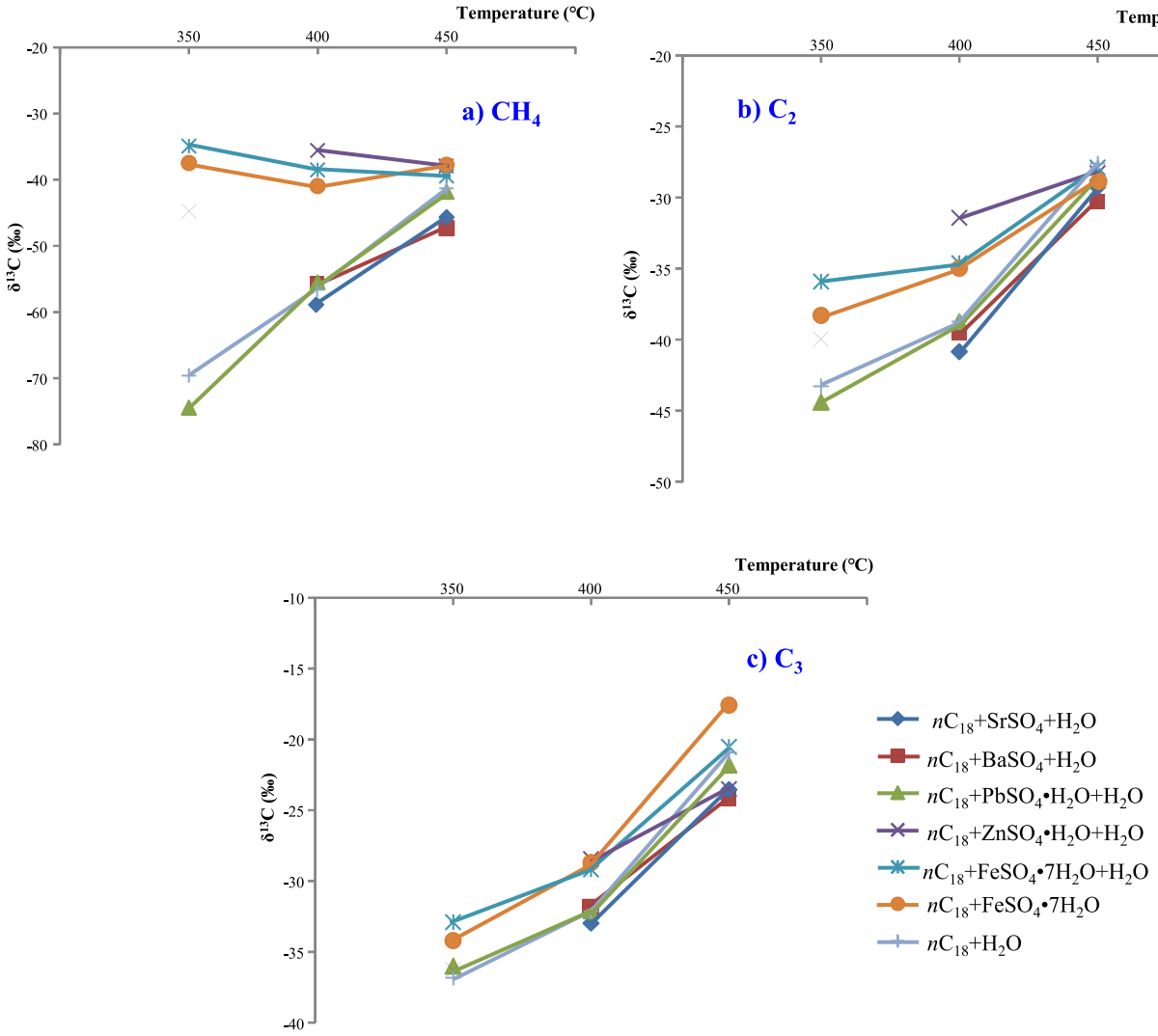

Fig. 2. Carbon isotopic compositions of C_1-C_3 produced in $FeSO_4{\cdot}7H_2O$, $ZnSO_4{\cdot}H_2O$, $SrSO_4$, $BaSO_4$, $PbSO_4{\cdot}H_2O$ and the blank series at 300 °C, 350 °C 400 °C and 450 °C, respectively, for 72 h.

ture and the relatively low Gibbs free energy of reaction (Machel, 2001), and liquid hydrocarbons remained at these temperature conditions. Even so, we could not completely exclude the occurrence of CH_4 oxidation in the TSR. The results of some case-studies and simulation experiments (Worden and Smalley, 1996; Cai et al., 2003, 2013; Heydari, 1997; Pan et al., 2006; Lu et al., 2012) supported the possibility of CH_4 oxidation in methane-dominated TSR (with high C_1/C_{1-6} ratios, even > 0.95 in some cases) where methane is the main reactant. Moreover, Worden and Smalley (2004) even showed that methane concentration decreases to a higher extent than the other alkane gas concentrations and highlighted that CH_4 and C_2 + gases undergo a similar increase in $\delta^{13}C$, suggesting that both have similar reactivity during TSR. Thus, it is possible for the occurrence of slight $^{12}CH_4$ oxidation by TSR in the $FeSO_4$ (350–400 °C) and the $ZnSO_4$ series (400 °C) resulting in an increased $\delta^{13}C$ of the methane with low yields. As some simulation experiments showed that hematite (Fe_2O_3) could oxidize the methane in the absence of water (Kiyosu and Krouse, 1989; Kiyosu and Imaizumi, 1996), we speculate that Fe^{3+} might be produced at 350 °C and 400 °C in the $FeSO_4$ experiments and play an important role to the CH_4 oxidation.

At 350–400 °C, the pyrolysis experiments separate into two groups based on $\delta^{13}C$ of the C_1–C_3 products (Fig. 2, Table 2). The $FeSO_4$ and $ZnSO_4$ series were classified as one group, in which the $\delta^{13}C$ values of the C_1–C_3 products were altered by TSR and heavier than that of products in the control series. Other metal sulfate series group together, where the $\delta^{13}C$ values of their C_1–C_3 products were close to the control series and not altered by TSR. At 450 °C (Fig. 2, Table 2), the $\delta^{13}C$ of methane in the $FeSO_4$ and $ZnSO_4$ experiments was slightly heavier than that of methane in the other metal sulfate and control experiments. The $\delta^{13}C$ values of C_2–C_3 in all the pyrolysis experiments were close to each other and had no apparent trends (Fig. 2, Table 2), mainly because the majority of heavy hydrocarbons are pyrolyzed at this temperature, leading to positive shifts of the C_1–C_3 gas products. Eventually, $\delta^{13}C$ values became closer to that of the precursor n-C_{18} (−25.3‰) and the influence of isotopic fractionation from TSR would become smaller.

3.1.4. Comparison of TSR reactivity of different metal sulfates

Based on the gas yields and carbon isotopic data, we conclude that $FeSO_4$ was the most reactive sulfate for TSR among the examined metal sulfates, with the initiating temperature below 350 °C or even 300 °C, similar to $MgSO_4$ as previously reported (Zhang et al., 2008b; Lu et al., 2011). The TSR initiation temperature of the $ZnSO_4$ series was estimated to be above 350 °C. TSR initiation temperature with $SrSO_4$ and $BaSO_4$ was > 400 °C, and with $PbSO_4$ it must be > 450 °C. The order of TSR reactivity of metal sulfates was therefore assessed as $FeSO_4$ > $ZnSO_4$ > $SrSO_4$, $BaSO_4$ > $PbSO_4$.

Since water is supercritical at 400 °C and 450 °C (T > 375 °C, P > 22 MPa), the initiation temperatures of TSR in $ZnSO_4$, $SrSO_4$, and $BaSO_4$ series would be influenced by the activation of supercritical water. These metal sulfates might not initiate the TSR in nature, as supercritical water seldom exists in conventional geological environments. Thus, $FeSO_4$ would be most reactive for TSR among the MVT minerogenetic metal sulfates. It might be responsible for the initiation and activation of the TSR during the MVT ore deposit formation.

3.2. TSR of $FeSO_4$ with n-C_{18}

3.2.1. Liquid and solid products and their formation

3.2.1.1. Liquid hydrocarbons. The extracts of the $FeSO_4$ series at 300 °C and 350 °C (72 h) contained mainly residual n-C_{18}, with trace amounts of $C_{9\text{-}15}$ n-alkanes/alkenes from cracking of n-C_{18}; hence, hydrocarbon cyclization and aromatization was not evident. We therefore focused on the 400 °C and 450 °C products of the $FeSO_4$ series. The $PbSO_4$ and the control series had no TSR occurrence and were regarded as controls for the investigation of the TSR influence on hydrocarbon pyrolysis and the formation/evolution of aromatic and sulfur compounds.

At 400 °C, the extracts from the $PbSO_4$ and the control experiments contained mainly residual n-C_{18} and minor amounts of smaller n-alkanes from thermal cracking of n-C_{18}; no aromatic products were detected (Fig. 3a, c). At 450 °C, n-alkanes disappeared and large amounts of aromatic hydrocarbons (naphthalenes, phenanthrenes, fluorenes, pyrenes and benzo-fluorenes) were detected (Fig. 3b, d). These aromatic hydrocarbons originate from the cyclization and aromatization of the smaller alkyl moieties initially cleaved from n-C_{18}.

The extracts of $FeSO_4$ pyrolysis at 400 °C contained mainly aromatic hydrocarbons, such as alkylbenzenes (AB), naphthalene and alkylnaphthalenes (N, MN, DMN, TMN), phenanthrene and alkylphenanthrenes (P, MP, DMP), fluorene and methylfluorenes (F, MF), biphenyl (BP), and dibenzofuran (DBF), as well as low amounts of residual alkanes, low amounts of dibenzothiophene (DBT) and elemental sulfur (S_8) (Fig. 3e). These S-products, particularly S_8, and other aromatic products (e.g., BP, DBF) were detected in high abundance at 450 °C (Fig. 3f). No n-alkanes were detected, implying their complete TSR utilization.

Compared with $PbSO_4$ and the control series, $FeSO_4$ exhibited lower temperatures for the formation of the aromatic hydrocarbons, indicating that TSR facilitated the decomposition of n-C_{18} for the production of the aromatic hydrocarbons. Aromatic hydrocarbons (naphthalenes, phenanthrenes, fluorenes, pyrenes and benzo-fluorene) are derived from the decomposition of n-C_{18} and subsequent cyclization and aromatization.

Elemental sulfur and organic sulfur compounds (OSCs) were detected in the solvent extractable pyrolysates. They are common TSR products generated by H_2S reacting with organic compounds (Orr et al., 1977; Krouse et al., 1988). Elemental sulfur can also be produced by the reaction of H_2S with dissolved sulfate (Krouse et al., 1988; Machel et al., 1995; Machel, 2001; Heydari, 1997) and thermal degradation of pyrite (Wiltowski et al., 1987; Lambert et al., 1998; Bhargava et al; 2009; Huang et al., 2015). Based on the H_2S yields of the $FeSO_4$ series, DBT likely formed from the reaction of H_2S with fluorene, while S_8 was produced by the reaction of H_2S and HSO_4^- (as described in Section 3.1.1). BP and DBF were only present in the $FeSO_4$ series along with DBT and could be produced from desulfurization and oxidation of DBT.

The formation of aromatic hydrocarbons, DBT and S_8 at 400 °C and 450 °C in the $FeSO_4$ series could be expected. However, no thiophenic and sulfidic compounds were produced at 300 °C and 350 °C. These results are inconsistent with the field and laboratory TSR simulation experiments at 300 °C and 350 °C without iron sulfate, which were reported to have abundant thiophenic and sulfidic compounds (Manzano et al., 1997; Cai et al., 2003; Zhang et al., 2008a). We attribute this to H_2S produced at 300 °C and 350 °C in the $FeSO_4$ series preferentially reacting with Fe^{2+} (Eqns 1–2), limiting the amount of H_2S reacting with the organic compounds to produce OSCs. The H_2S yield increased with increasing temperatures (400–450 °C) and the TSR rate accelerated. At these temperatures, labile OSCs formed from the H_2S incorporate into organic compounds which are thermally unstable and only the more stable compounds, such as DBT and element sulfur, will persist.

3.2.1.2. Iron mineral formation and its implication for the TSR initiation. Data on the solid products for the $FeSO_4$ series are listed in Table 3. High abundances of ferrous sulfate (70%–95%) remained after the pyrolysis of $FeSO_4{\cdot}7H_2O$ at 300 °C and 350 °C, indicating incomplete reaction of the reactant. The major

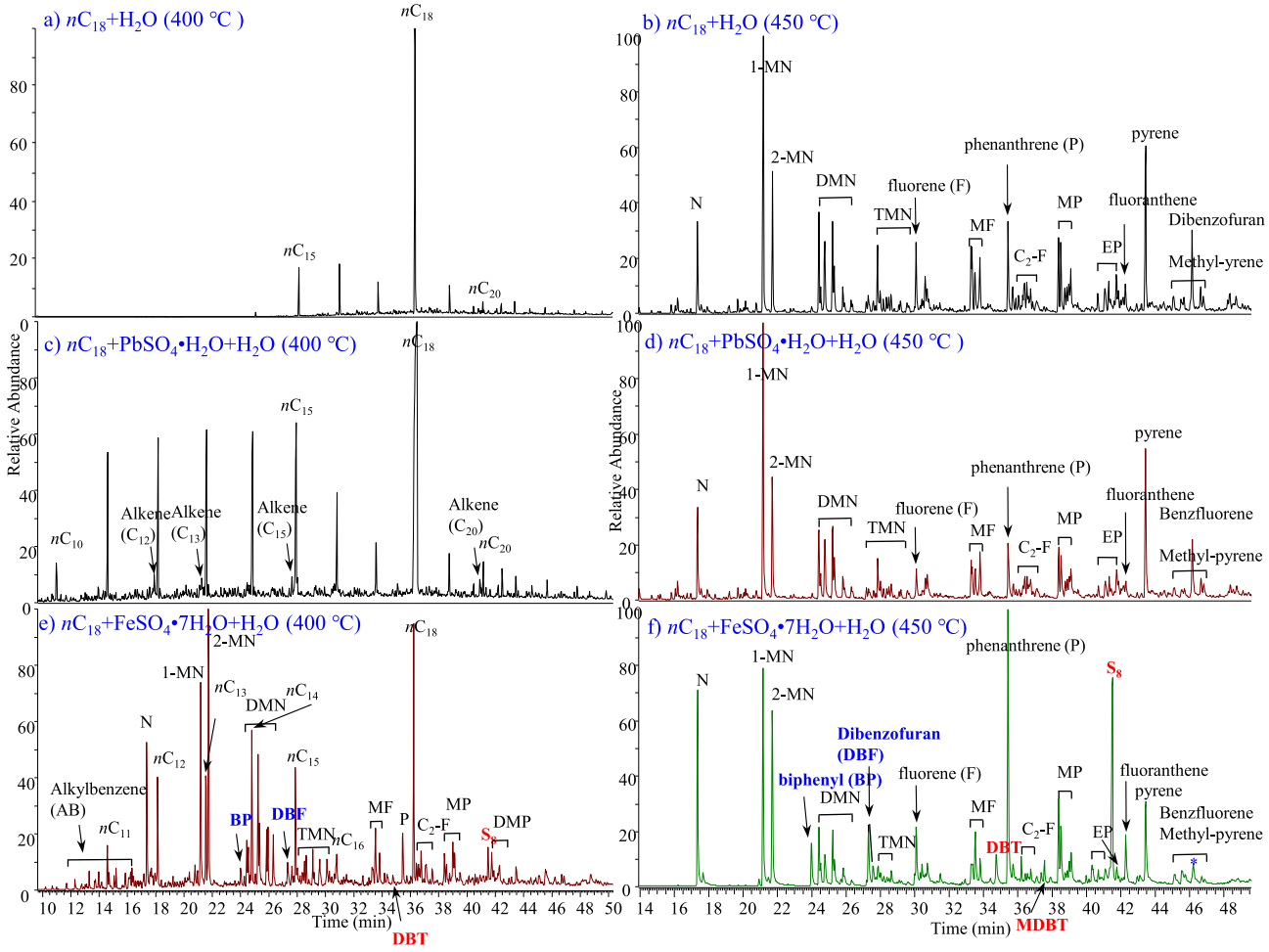

Fig. 3. GC–MS analysis of the solvent extractable fractions of residues from the control experiments at 400 °C (a) and 450 °C (b), the $PbSO_4$ pyrolysis experiments at 400 °C (c) and 450 °C (d), and the $FeSO_4$ pyrolysis experiments at 400 °C (e) and 450 °C (f) for 72 h.

Table 3
Residual solids and their relative abundance in $FeSO_4{\cdot}7H_2O$ and n-C_{18} pyrolysis experiments, analyzed by XRD.

Temperature (°C)	Time (D)	H_2O	Reactant ($FeSO_4$)	Magnetite (Fe_3O_4)	pyrite (S^-) (FeS_2)	Pyrrhotite (S^{2-}) ($Fe_{1-x}S$, Fe/S = 0–0.17)	Geothite (α-FeO(OH))
300	3	+	81.4%	0	18.6%	0	0
300	3		94.9%	0	5.1%	0	0
350	3	+	92.8%	0	7.2%	0	0
350	3		92.0%	0	8.0%	0	0
350	15		73.2%	12.4%	14.3%	0	0
400	3	+	21.9%	9.8%	19.2%	27.6%	21.5%
400	3		21.5%	12.3%	12.7%	34.7%	18.8%
450	3	+	27.1%	8.4%	0	35.5%	29.0%
450	3		23.8%	7.5%	0	45.2%	23.6%
450	15		0	18.1%	0	66.2%	15.7%

product of the ≤ 350 °C pyrolysis was pyrite (FeS_2). Considerably more ferrous sulfate was consumed at 400 °C, but with only a slight increase in pyrite. Significant new products at this temperature include magnetite (Fe_3O_4, 9.8%), pyrrhotite ($Fe_{1-x}S$, Fe/S = 0–0.17, 27.6%) and goethite (α-FeO(OH), 21.5%). At 450 °C, the yield of pyrite decreased to zero along with the disappearance of $FeSO_4$, while the yields of $Fe_{1-x}S$ and α-FeO(OH) increased (Fig. 4).

Pyrite is one of the most abundant iron sulfides on Earth and is a key component of both sulfur and iron geochemical cycles (Schoonen and Barnes, 1991). Berner (1984) recognized that pyrite formed during shallow burial processes via the reaction of detrital iron minerals with H_2S. Based on field observations and experimental studies, Schoonen and Barnes (1991) subsequently proposed the following two-step reaction process: (1) Initial precipitation of iron monosulfide (FeS) which then reacts with aqueous hydrogen sulfide (HS^-) and ferrous iron (Fe^{2+}) (Eq. (1)), and (2) Further reduction of iron disulfide from iron monosulfide precursors (Eq. (2)) (Drobner et al., 1990; Rickard, 1997; Truche et al., 2009; Fu et al., 2016). Hence, the detection of pyrite at low pyrolysis temperature (≤350 °C) reflects the TSR production of H_2S and its subsequent reaction with Fe^{2+}.

$$Fe^{2+} + H_2S \rightarrow FeS + 2H^+ \quad (1)$$

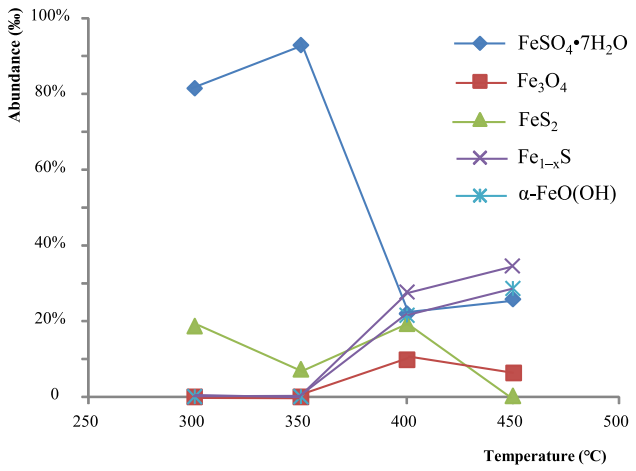

Fig. 4. XRD analysis of residual solids in $FeSO_4{\cdot}7H_2O$ series at 300 °C, 350 °C, 400 °C and 450 °C for 72 h (quartz might come from the pollution of a small amount of standard sample).

$$H_2S + FeS \rightarrow FeS_2 + H_2 \quad (2)$$

Two routes might account for the production of pyrrhotite. One is the reaction of magnetite (Fe_3O_4) and volatile sulfur (Eq. (3)) (Tauson and Sapozhnikov (2005)). This process also produces SO_2, which is not presently detected in the gas products and thus unlikely to have occurred here. The second possible formation pathway involves the thermal transformation (Eq. (4)) of pyrite (Fe/S = 0.5) to pyrrhotite (Fe/S < 0.17), which can result in a significant release of sulfur (Wiltowski et al., 1987; Lambert et al., 1998; Bhargava et al; 2009; Huang et al., 2015). This process may account for the high concentrations of elemental sulfur detected in the solvent extractable fraction of the residues from ≥400 °C pyrolysis.

$$(1-x)\ Fe_3O_4 + (5-2x)\ S \rightarrow 3Fe_{1-x}S + 2_{(1-x)}SO_2 \quad (3)$$

$$FeS_2 \rightarrow Fe_{1-x}S + S \quad (4)$$

The absence of pyrite at 450 °C (Table 3) provided strong evidence for the thermal degradation of pyrite, which has been demonstrated in the controlled thermal decomposition of FeS_2 to $Fe_{1-x}S$ and S^0 in an inert (Ar) atmosphere at temperatures in excess of 500 °C (Coats and Bright, 1966; Bhargava et al., 2009). Similar thermal experiments showed that addition of H_2 or H_2O reduced the activation temperature for pyrite degradation to ~450 °C (Wiltowski et al., 1987; Lambert et al., 1998; Huang et al., 2015). Moreover, in the thermal experiment under a CO_2 atmosphere conducted by Bhargava et al. (2009), pyrite began to be transformed into pyrrhotite at a temperature of 400 °C. This temperature corresponds to conditions at which pyrrhotite was produced in our $FeSO_4$ experiment. Thus, pyrrhotite in the $FeSO_4$ series was probably generated from thermal degradation of pyrite.

The production of magnetite indicated an availability of both Fe^{2+} and Fe^{3+}. Industrial preparations of Fe_3O_4 nanoparticles make use of both ferrous and ferric salt reagents (Feltin and Pileni, 1997; Wei et al., 2012; Aghazadeh et al., 2017). Some of the Fe^{2+} from the thermal dissolution of $FeSO_4$ (not consumed by H_2S) may be oxidized to Fe^{3+} by HSO_4^- (Eq. (10)). Magnetite (12.4%; Table 3) was detected at the 350 °C pyrolysis temperature applied over the longer 15 days (360 h), indicating that Fe^{3+} can be generated at this lower pyrolysis temperature. The subsequent reaction of H_2O and Fe^{3+}, as expressed by Eq. (5) (Fu et al., 2016), might account for the production of goethite (α-FeO(OH)), which was observed in the 400 °C and 450 °C residues.

$$Fe^{3+} + 2H_2O \rightarrow FeO(OH) + 3H^+ \quad (5)$$

3.2.2. Initiated mechanism for the TSR of $FeSO_4{\cdot}7H_2O$ series

SO_4^{2-} is the oxidizing agent of the TSR, but direct reduction of sodium sulfate by hydrocarbons does not significantly occur below 800 °C (Goldstein and Aizenshtat, 1994). Tang et al. (2005) and Zhang et al. (2007, 2008a) proposed an initiating stage for TSR and speculated that HSO_4^- and sulfates form contact ion pairs (CIP) as the main SO_4^{2-}-type-oxidant for hydrocarbon oxidation and TSR initiation under laboratory and natural conditions, respectively. Calculations by Ma et al. (2008) indicated that the activation energy required to reach the transition state for the interaction of SO_4^{2-} with ethane was 78 kcal/mol, significantly higher than the 54 kcal/mol calculated for the activation energy required for interaction of HSO_4^- with ethane. Ma et al. (2008) contended that the tetrahedral molecular symmetry (Td), nearly spherically symmetrical electron density and the highest occupied molecular orbital (HOMO), made SO_4^{2-} unreactive. Dissolved SO_4^{2-} would therefore be largely unreactive without any catalytic assistance. He et al. (2014) suggested the more reactive HSO_4^- was the dominant TSR oxidant in hydrous pyrolysis experiments (>300 °C), whereas the most feasible TSR oxidant in the subsurface is CIP, which had a considerable concentration in the formation water at reservoir temperatures (<250 °C). Based on these viewpoints for TSR and our experimental data, we will discuss the initiated mechanism for the TSR which occurred in the $FeSO_4{\cdot}7H_2O$ experiments.

TSR occurred at 300 °C in the $FeSO_4{\cdot}7H_2O$ experiment (72 h), indicating HSO_4^- and/or $[FeSO_4]_{CIP}$ are possible triggers to initiate TSR. As with the formations of $[MgSO_4]_{CIP}$ and $[CaSO_4]_{CIP}$ proposed by Ma et al. (2008), $[FeSO_4]_{CIP}$ might be produced by combination of Fe^{2+}, SO_4^{2-}, and H_2O at low temperature (≤300 °C), while HSO_4^- could come from reaction of H^+ and SO_4^{2-} (Eq. (7)). The concentration of HSO_4^- mainly depends on the concentration of H^+, as the initial loading of $FeSO_4$ is in excess. Combination of Fe^{2+}, SO_4^{2-}, and H_2O might produce ferrous hydroxide-sulfate-hydrate complex (FHSH), release H^+ and subsequently form HSO_4^-, according to Eq. (9) at temperature below 300 °C, just as $MgSO_4$ does, as described by Ma et al. (2008). In the pyrolysis of a 0.08 mol/L solution of $FeSO_4{\cdot}7H_2O$, Perkins et al. (2016) found acidic conditions (*pH* = 3.5) at room temperature. Thus, in our TSR simulation experiment at 300 °C, the *pH* might have decreased to 3.5 with the hydrolysis of Fe^{2+}. HSO_4^- produced at such acidic conditions can initiate TSR with no catalysis of reduced sulfur (Zhang et al., 2008a). It therefore seems plausible that the concentration of HSO_4^- produced at a temperature as low as 300 °C in $FeSO_4$ experiments might be enough to initiate TSR.

$$(1-x)\ FeS_2 \rightarrow Fe_{1-x}S + (1-2x)\ S \quad (6)$$

$$H^+ + SO_4^{2-} \rightarrow HSO_4^- \quad (7)$$

$$2\ Mg^{2+} + 3H_2O + SO_4^{2-} \rightarrow Mg(OH)_2{:}MgSO_4{:}H_2O + 2H^+ \quad (8)$$

$$2Fe^{2+} + 3H_2O + SO_4^{2-} \rightarrow Fe(OH)_2{:}FeSO_4{:}H_2O + 2H^+ \quad (9)$$

3.2.3. Constraints on the rate of $FeSO_4$-type TSR

Sulfur-containing carriers containing sulfate, HSO_4^-, H_2S, elemental sulfur, other inorganic sulfur species and OSCs, are all considered to be important to the initiation and catalysis of TSR. TSR was apparently accelerated at 350–450 °C in the $FeSO_4$ experiments. Based on the analyses of gaseous, liquid and solid products in the $FeSO_4$ experiments and the chemical properties of $FeSO_4$, we proposed several constraints on the formation of sulfur-containing carriers and the rate of $FeSO_4$-type TSR.

3.2.3.1. Concentrations of H^+ and HSO_4^-. Zhang et al. (2012) found in $CaSO_4$ pyrolysis experiments that the initial *pH* could evidently affect TSR rate. Since *pH* is related to the concentration of H^+, namely the HSO_4^- concentration, HSO_4^- might be, not only the initiator, but also a reactive reactant in TSR.

The water content of the system can also affect the concentrations of FHSH and H^+ (Eq. (9)). In the $FeSO_4{\cdot}7H_2O$ series with no added water, the dehydration of the $FeSO_4{\cdot}7H_2O$ reactant at > 290 °C provides H^+ for the formation of HSO_4^- (Pelovski et al., 1996; Zboril et al., 2002). Rozenite ($FeSO_4{\cdot}4H_2O$) is produced at first, followed by szomolnokite ($FeSO_4{\cdot}H_2O$). The lack of water in the gold tube system would obviously constrain initial formation rates of H^+ and HSO_4^- and the final HSO_4^- concentration. So, the concentration of HSO_4^- in the $FeSO_4{\cdot}7H_2O$ series without adding H_2O should be different from the $FeSO_4{\cdot}7H_2O$ series with H_2O at different temperatures.

Experiments of $FeSO_4{\cdot}7H_2O$ and n-C_{18} pyrolysis with and without added H_2O were conducted to examine if the concentration of HSO_4^- in $FeSO_4$ pyrolysis experiment could also affect the TSR rate. By comparing the yields of gases produced in the two series, we found that yields of organic C_1–C_5 and inorganic CO_2 and H_2S in series with additional H_2O were higher than those of gases produced in the series without adding more H_2O. The gaps of gas yields at 300 °C and 350 °C were not evident in Fig. 5 due to low yields; H_2S yields in both series decreased to zero at 450 °C as a lone exception. (Fig. 5, Table 1). We speculate that the TSR rate in the series with added H_2O might be higher than that in series without H_2O, i.e. an increase in HSO_4^- concentration accelerates the TSR rate in $FeSO_4$ series. Thus, increase of H^+ concentration could generate protonated sulfate ion HSO_4^- and play a key role for TSR initiating and reactive reactant in the $FeSO_4$ experiments.

3.2.3.2. Valence change of iron. Fe^{2+} and Fe^{3+} are common valences of iron, with Fe^{2+} easily oxidized to Fe^{3+}. As magnetite was produced in the $FeSO_4$ experiment at 350 °C for 360 h, Fe^{2+} had been partly oxidized to Fe^{3+} by HSO_4^- during TSR (Eq. (10)). It is well known that Fe^{3+} has a strong affinity for water initiating a series of hydrolysis that release H^+ (Eqs. (11)–(13)) and can lead to the iron-hydroxide-sulfate-hydrate complex (IHSH) formation (Eq. (14)), which would greatly increase the concentration of HSO_4^-, and promote TSR. These reactions are in accordance with the fact that TSR were greatly accelerated at 350–450 °C in $FeSO_4$ series.

$$8Fe^{2+} + HSO_4^- + 5H_2O \rightarrow 8Fe^{3+} + H_2S + 9OH^- \quad (10)$$

$$Fe^{3+} + H_2O \rightarrow FeOH^{2+} + H^+ \quad (11)$$

$$FeOH^{2+} \text{ and } Fe(OH)_2^+ + H_2O \rightarrow Fe(OH)^+_2 + H^+ \quad (12)$$

$$Fe(OH)_2^+ + H_2O \rightarrow Fe(OH)_3 + H^+ \quad (13)$$

$$3Fe^{3+} + 4H_2O + 3SO_4^{2-} \rightarrow Fe(OH)_3{:}Fe_2(SO_4)_3{:}H_2O + 3H^+ \quad (14)$$

Thus, the Fe(II)-Fe(III) valence range and strong hydrolysis properties of Fe^{3+} likely accounts for the relatively high TSR character of $FeSO_4$ observed in the pyrolysis simulations.

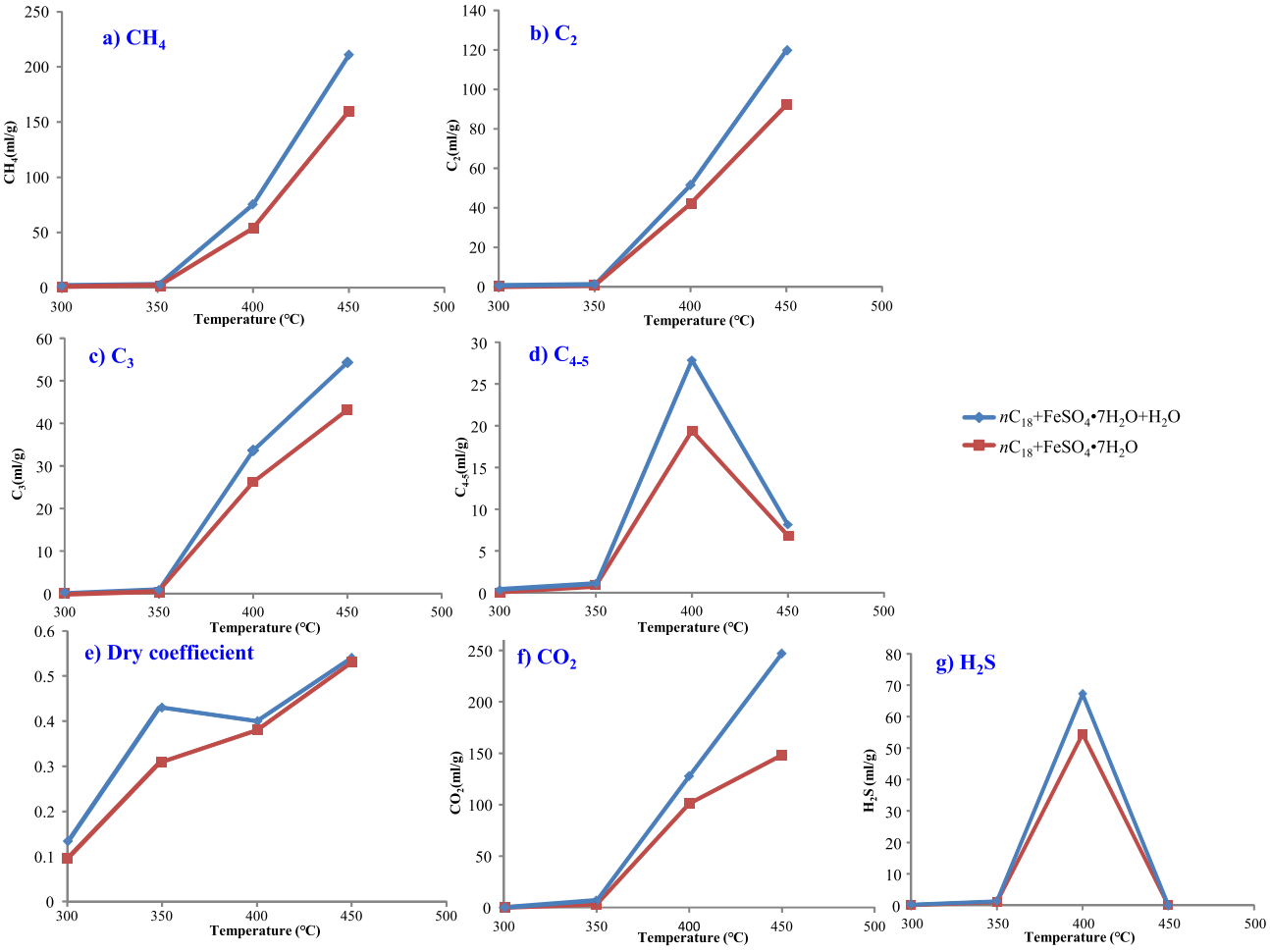

Fig. 5. Comparison of the gas yields of C_1–C_5, CO_2 and H_2S and dry coefficient in $FeSO_4{\cdot}7H_2O$ pyrolysis experiments with and without water at 350 °C, 400 °C, 450 °C for 72 h.

3.2.3.3. Effect of FeS_2 precipitation on the TSR rate. Many previous laboratory TSR simulation experiments proposed that H_2S, elemental sulfur and labile organic sulfur compounds (LSC) could initiate and promote TSR, and used them as reduced sulfur catalysis in the simulation experiments (Zhang et al., 2008a; Amrani et al., 2008). H_2S could react freely with hydrocarbons and produce various organic sulfides (e.g., thiol, thiophene and benzothiophene; Lu et al., 2013). It could also react with inorganic SO_4^{2-} to form inorganic sulfur compounds with intermediate valence states, such as elemental sulfur, polysulfide, sulfide and thiosulfate (Eqs. (15) and (16)). Elemental sulfur is also regarded as an initiating agent of TSR (Truche et al., 2014). Elemental sulfur easily yields sulfur free radicals at temperatures as low as 100 °C (Toland, 1960; Orr and Sinninghe Damsté, 1990), which could accelerate hydrocarbon oxidation, producing H_2S and HCO_3^- (Eqs. (17) and (18)) that then promote TSR (Cross et al., 2004; Amrani et al., 2008; Zhang et al., 2012; Lu et al., 2012). Amrani et al. (2008) proposed that LSC produced in the early stage of TSR was more reactive than inorganic sulfur (elemental sulfur and H_2S), and a small number of LSC could greatly accelerate TSR. LSCs can be produced by reaction of H_2S/elemental sulfur with hydrocarbons (Schmid et al., 1987; Stoler et al., 2003; Amrani et al., 2006). So H_2S, S_8 and LSCs are interconvertible to each other as intermediates and catalysts of TSR.

$$HSO_4^- + 3H_2S + H^+ \rightarrow 4S^o + 4H_2O \quad (15)$$

$$SO_4^{2-} + 3H_2S + 2H^+ \rightarrow 4S^o + 4H_2O \quad (16)$$

$$4S^o + 1.33(-CH_2-) + 2{\cdot}66H_2O + 1.33OH^- \rightarrow 4H_2S + 1.33HCO_3^- \quad (17)$$

$$4S^o + 1.33(-CH_2-) + 2{\cdot}66H_2O \rightarrow 4H_2S + 1.33CO_2 \quad (18)$$

The yield of H_2S produced in gold-tube system for $FeSO_4$ series at 300–350 °C was so low that LSC and elemental sulfur could not form. The precipitation of FeS_2 at this temperature range consumes large amounts of H_2S produced by TSR and there is little left to react with hydrocarbons and HSO_4^- to produce LSC and elemental sulfur. Hence, at 300–350 °C, FeS_2 precipitation would reduce the generation of sulfur-containing carriers (H_2S, OSCs and elemental sulfur), and limit the increase of TSR rate.

3.3. The TSR behavior of minerogenetic metal sulfates in fluids of MVT ore deposits

$FeSO_4$, $ZnSO_4$, $PbSO_4$, $BaSO_4$, and $SrSO_4$ are all associated with the basin brines for mineralization of MVT ore deposits. The present pyrolysis experiments of these metal sulfates with *n*-C_{18} provide insights into their relative TSR behavior and role in the formation of the MVT ore deposit.

MVT mineral deposits are typically carbonate hosted (mainly calcite $CaCO_3$, followed by dolomite $MgCO_3$), strata-bound metal sulfide bodies (sphalerite, galena, pyrite and marcasite) that occur as both open-space fillings and replacements of the host rocks (Anderson, 1988). Fluid erosion of the hosted carbonate rocks, TSR and mineralization (precipitation and formation of sphalerite, galena, pyrite, and marcasite) can occur simultaneously. The metal content of ore fluids typically include Fe^{2+}, Zn^{2+}, Pb^{2+}, Sr^{2+}, Ba^{2+}, SO_4^{2-}, Ca^{2+} and lesser amounts of Mg^{2+} formed from erosion of carbonate rocks. Transported hydrocarbons in fluids were also included in the reducing agents of the TSR. MVT deposits typically contain significant quantities of bitumen, pyrobitumen, or liquid petroleum (Sverjensky, 1986; Gregg, 2004; Gregg and Shelton, 2012) which may be secondary products of TSR. During MVT mineralization, as the dissolution of hosted carbonate rocks by fluid occurs, the hydrocarbons should have reacted with HSO_4^- and CIP and initiated TSR, resulting in the formation of H_2S, and precipitation of sphalerite, galena, pyrite and filling in the surrounding rocks.

CIP and HSO_4^- in the ore fluid of MVT systems might play a significant role for initiating TSR. Since no TSR occurred in the gold-tube simulation experiments of $PbSO_4$, $BaSO_4$, and $SrSO_4$ at 350 °C, effects of Pb^{2+}, Sr^{2+} and Ba^{2+} on the formation of CIP and HSO_4^- are likely negligible. Sr^{2+} and Ba^{2+} quickly precipitates with SO_4^{2-} and celestine ($SrSO_4$) and barite ($BaSO_4$) ores would be formed after being transported by the fluid. Ca^{2+} is definitely abundant in the fluids, but $CaSO_4$ reduction with hydrocarbons at 330 °C was found hard to occur without catalysis of any reduced sulfur. Previously, the TSR rate of $CaSO_4$ pyrolysis was shown to be extremely slow, even with increasing H_2S loading at a *pH* of about 5.0 (Zhang et al., 2008a). Ca^{2+} is therefore unlikely significantly to influence the TSR of MVT systems. In the pyrolysis experiments at low temperature (<350 °C), TSR occurred in the presence of $FeSO_4$ and $MgSO_4$, i.e. Fe^{2+} and Mg^{2+} may both account for enough CIP and HSO_4^- to initiate TSR, during the dissolution of surrounding carbonate rocks by fluid. The present TSR pyrolysis simulations also suggest $ZnSO_4$ can support TSR, but not near the same capacity as $FeSO_4$.

In the previous $MgSO_4$ experiment (Zhang et al., 2008b), the CO_2 and H_2S yields produced at low temperature (<350 °C) (especially for H_2S) were higher than measured here produced in the $FeSO_4$ series, indicating the effects of Mg^{2+} on initiating TSR in MVT mineralization could be greater than Fe^{2+}. The formation of FeS_2 in the $FeSO_4$ series at low temperature (<350 °C) consumes most of the H_2S produced and restrained the TSR rate increase. This effect is not seen in the $MgSO_4$ experiments that H_2S yield would increase in the gold-tube reactor as no metal sulfide precipitates to consume H_2S. LSC and element sulfur would be produced by H_2S and greatly promote the TSR. In MVT mineralization, vast quantities of insoluble metal sulfides (pyrite, gelenite and sphalerite) are formed, in accordance with $FeSO_4$ simulation experiments but different from $MgSO_4$ experiments. Hence, the effects of Mg^{2+} on TSR in the MVT mineralization might be not as great as seen in the simulation experiments.

Although our simulation experiments showed that $PbSO_4$ and $ZnSO_4$ reduction does not occur at low temperatures (<350 °C), the H_2S or/and S^{2-} produced by Fe^{2+} and HSO_4^- in the fluid in the process of MVT mineralization reacts with brines and forms PbS, ZnS, and FeS_2 precipitation. Hence, the mineralization for MVT ore deposit might be initiated TSR by Fe^{2+}, HSO_4^- and produced H_2S. After the initiation of the TSR, Fe^{3+} from the oxidation of Fe^{2+} significantly accelerates the TSR by forming ferric hydroxide-sulfate-hydrate complex (Eq. (14)), largely increasing the concentrations of H^+ and HSO_4^- in the fluid. The Fe^{3+} might act as a buffer, which could maintain an in-situ low *pH*, keeping the supply and the consumption of HSO_4^- in the brine, and leading to TSR occurring continuously and constantly, which is consistent with the reconstructed low *pH* in the Pillara MVT fluid inclusion (*pH* 1.7–3.8; Hurtig et al., 2018) and the Illinois-Kentucky MVT fluid inclusion (*pH* 0–1.4; Kenderes and Appold, 2017). Thus, H_2S would be produced continuously and contribute to large and super-large scales of MVT ore deposits.

4. Conclusions

A series of isothermal gold-tube hydrous-pyrolysis experiments involving $PbSO_4{\cdot}H_2O$, $ZnSO_4{\cdot}H_2O$, $FeSO_4{\cdot}7H_2O$, $SrSO_4$, $BaSO_4$ and *n*-C_{18} were carried out in this study. The pyrolysis gas products analyzed by GC and GC-irMS, as well as the residual liquid hydrocarbon products and residual solids analyzed by GC–MS and XRD, were used to discuss the TSR behaviors of the MVT minerogenetic

metal ions (Pb^{2+}, Zn^{2+}, Fe^{2+}, Sr^{2+}, Ba^{2+}) under laboratory conditions. TSR behaviors of these minerogenetic metal ions in formation of the MVT ore deposit were intensively investigated and the principal findings of this study are summarized below:

(1) The TSR reactivity of the sulfates was identified to be in the order: $FeSO_4$ > $ZnSO_4$ > Sr/$BaSO_4$ > $PbSO_4$. Accordingly, the pyrolysis temperature at which TSR was initiated was 300 °C for $FeSO_4{\cdot}7H_2O$; 400 °C for $ZnSO_4{\cdot}H_2O$; 450 °C for $SrSO_4$ and $BaSO_4$, whilst no TSR was observed with $PbSO_4$ even at the highest pyrolysis temperature of 450 °C.
(2) Pyrite was produced at 300 °C in the $FeSO_4{\cdot}7H_2O$ experiment, which indicated a low initiating temperature for TSR (<300 °C) and was in accordance with the data for the gaseous products. The formation of magnetite and goethite indicated Fe^{2+} was oxidized to Fe^{3+} during TSR.
(3) TSR occurred at low temperature in the $FeSO_4{\cdot}7H_2O$ experiment and is attributed to two factors: formation of H^+ and HSO_4^- and oxidation of Fe^{2+} to Fe^{3+}. The hydrolysis of Fe^{2+} or the formation of ferrous hydroxide-sulfate-hydrate complex could have increased the concentration of H^+ and HSO_4^-, which lowered the initiating temperature of the TSR. Hydrolysis of Fe^{3+} or the formation of iron hydroxide-sulfate-hydrate complex greatly increased the concentrations of H^+ and HSO_4^- and formed mineral buffer for the TSR.
(4) In consideration of dolomite (containing Mg^{2+}, Fe^{2+} and Mn^{2+}) and the vast amount of pyrite associated with MVT ore deposits, we propose that $FeSO_4$ has a similar behavior to $MgSO_4$ and accelerates the initiation of TSR by forming contact ion pairs and HSO_4^- in the brine fluid. After the initiation of the TSR, the produced H_2S would quickly precipitate with Fe^{2+}, Zn^{2+}, Pb^{2+} as metal sulfides. Although there is no catalysis effect of reduced sulfur (H_2S), the Fe^{3+} (oxidized Fe^{2+} in the TSR) played a key role for maintaining the TSR. Hydrolysis or forming iron hydroxide-sulfate-hydrate complex greatly increased concentrations of H^+ and HSO_4^-, lowered the *pH* of the brine, and acted as a buffer for keeping low *pH* in-situ, leading to the continuous TSR occurrence.
(5) In our studies, TSR at low temperature (<350 °C) hardly occurred for Pb^{2+} and Zn^{2+}, but was easy for Mg^{2+} and Fe^{2+} considering the occurrence of pyrite and dolomite. Hence, $MgSO_4$ and $FeSO_4$ play significant roles in providing reduced sulfur and promoting TSR for the formation of large-scale MVT ore deposits.

Declaration of Competing Interest

The authors declare that they have no known competing financial interests or personal relationships that could have appeared to influence the work reported in this paper.

Acknowledgements

We thank Dr. Chenchen Shen for the technical and experimental assistance. HL acknowledges the financial support from National Major S&T Program of China [2017ZX05008-002-030], the Strategic Priority Research Program of the Chinese Academy of Sciences (XDA14010102), National Key Research and Development Project of China (2019YFC0605502), the GIG-135 Shale Gas Project, China (135TP201602), and Chinese NSF grants (41673066, 41673045, and 41973069); JL acknowledges the support of a Chinese NSF grant (41903064) and a Chinese Postdoctoral Science Foundation (2019M663131). We thank the Associate Editor and two reviewers for their very helpful comments to greatly improve the manuscript. This is contribution No. IS-2909 from GIGCAS.

Associate Editor–Clifford C. Walters

References

Abidi, R., Slim-Shimi, N., Somarin, A., Henchiri, M., 2010. Mineralogy and fluid inclusions study of carbonate-hosted Mississippi valley-type A in Allega Pb–Zn–Sr–Ba ore deposit, Northern Tunisia. Journal of African Earth Sciences 57, 262–272.

Aghazadeh, M., Karimzadeh, I., Ganjali, M.R., Behzad, A., 2017. Mn^{2+}-doped Fe_3O_4 nanoparticles: a novel preparation method, structural, magnetic and electrochemical characterizations. Journal of Materials Science: Materials in Electronics 28, 18121–18129.

Amrani, A., Said-Ahamed, W., Lewan, M.D., Aizenshtat, Z., 2006. Experiments on $\delta^{34}S$ mixing between organic and inorganic sulfur species during thermal maturation. Geochimica et Cosmochimica Acta 70, 5146–5161.

Amrani, A., Zhang, T., Ma, Q., Ellis, G.S., Tang, Y., 2008. The role of labile sulfur compounds in thermochemical sulfate reduction. Geochimica et Cosmochimica Acta 72, 2960–2972.

Anderson, G.M., 1975. Precipitation of Mississippi valley-type ores. Economic Geology 70, 937–942.

Anderson, G.M., 2008. The mixing hypothesis and the origin of Mississippi Valley-type ore deposits. Economic Geology 103, 1683–1690.

Anderson, G.M., Thom, J., 2008. The role of thermochemical sulfate reduction in the origin of Mississippi valley-type deposits. II. Carbonate-sulfide relationships. Geofluids 8, 27–34.

Anderson, R.C., 1988. Reconstruction of preglacial drainage and its diversion by earliest glacial forebulge in the upper Mississippi Valley region. Geology 16, 254–257.

Barton Jr, P.B., 1967. Possible role of organic matter in the precipitation of the Mississippi Valley ores. Economic Geology 3, 371–377.

Basuki, N.I., Taylor, B.E., Spooner, E.T.C., 2008. Sulfur isotope evidence for thermochemical reduction of dissolved sulfate in Mississippi Valley-type zinc-lead mineralization, Bongara area, northern Peru. Economic Geology 103, 783–799.

Berner, R.A., 1984. Sedimentary pyrite formation: an update. Geochimica et Cosmochimica Acta 48, 605–615.

Bhargava, S.K., Garg, A., Subasinghe, N.D., 2009. In situ high-temperature phase transformation studies on pyrite. Fuel 88, 988–993.

Cai, C.F., Worden, R.H., Bottrell, S.H., Wang, L.S., Yang, C.C., 2003. Thermochemical sulphate reduction and the generation of hydrogen sulphide and thiols (mercaptans) in Triassic carbonate reservoirs from the Sichuan Basin, China. Chemical Geology 202, 39–57.

Cai, C., Zhang, C., He, H., Tang, Y., 2013. Carbon isotope fractionation during methane-dominated TSR in East Sichuan Basin gasfields, China: A review. Marine and Petroleum Geology 48, 100–110.

Coats, A.W., Bright, N.F., 1966. The kinetics of the thermal decomposition of pyrite. Canadian Journal of Chemistry 44, 1191–1195.

Connan, J., Lacrampe-Couloume, G., Magot, M., 1995. Origin of gases in reservoirs. International Gas Research Conference, 21–61.

Cross, M.M., Manning, D.A.C., Bottrell, S.H., Worden, R.H., 2004. Thermochemical sulphate reduction (TSR): experimental determination of reaction kinetics and implications of the observed reaction rates for petroleum reservoirs. Organic Geochemistry 35, 393–404.

Drobner, E., Huber, H., Wächtershäuser, G., Rose, D., Stetter, K.O., 1990. Pyrite formation linked with hydrogen evolution under anaerobic conditions. Nature 346, 742.

Feltin, N., Pileni, M.P., 1997. New technique for synthesizing iron ferrite magnetic nanosized particles. Langmuir 13, 3927–3933.

Fu, Y., van Berk, W., Schulz, H.M., 2016. Hydrogen sulfide formation, fate, and behavior in anhydrite-sealed carbonate gas reservoirs: A three-dimensional reactive mass transport modeling approach. AAPG Bulletin 100, 843–865.

Galimov, E.M., 2006. Isotope organic geochemistry. Organic Geochemistry 37, 1200–1262.

Gregg, J.M., 2004. Mississippi Valley-type mineralization and the development of dolomite petroleum reservoirs. AAPG Annual Meeting 2004.

Gregg, J.M., Shelton, K.L., 2012. Mississippi Valley-type mineralization and ore deposits in the Cambrian–Ordovician great American carbonate bank. In: Derby, J.R., Fritz, R.D., Longacre, S.A., Morgan, W.A., Sternbach, C.A. (Eds.), The great American carbonate bank: The geology and economic resources of the Cambrian–Ordovician Sauk megasequence of Laurentia: AAPG Memoir 98, pp. 161–185.

Goldstein, T.P., Aizenshtat, Z., 1994. Thermochemical sulfate reduction: a review. Journal of Thermal Analysis and Calorimetry 42, 241–290.

Gorzawski, H., Fontboté, L., Field, C.W., Tejada, R., 1990. Sulfur isotope studies in the zinc-lead mine San Vicente, central Peru. Stratabound Ore Deposits in the Andes. Springer, Berlin, Heidelberg, pp. 305–312.

Heydari, E., 1997. The role of burial diagenesis in hydrocarbon destruction and H_2S accumulation, Upper Jurassic Smackover Formation, Black Creek Field, Mississippi. AAPG Bulletin 81, 26–45.

He, K., Zhang, S., Mi, J., Hu, G., 2014. The speciation of aqueous sulfate and its implication on the initiation mechanisms of TSR at different temperatures. Applied Geochemistry 43, 121–131.
Huang, F., Zhang, L., Yi, B., Xia, Z., Zheng, C., 2015. Effect of H_2O on pyrite transformation behavior during oxy-fuel combustion. Fuel Processing Technology 131, 458–465.
Hurtig, N.C., Hanley, J.J., Gysi, A.P., 2018. The role of hydrocarbons in ore formation at the Pillara Mississippi Valley-type Zn-Pb deposit, Canning Basin, Western Australia. Ore Geology Reviews 102, 875–893.
Janecky, D.R., Seyfried, W.E., 1983. The solubility of magnesium-hydroxide-sulfate-hydrate in seawater at elevated temperatures and pressures. American Journal of Science 283, 831–860.
Kesler, S.E., Appold, M.S., Martini, A.M., Walter, L.M., Huston, T.J., Richard Kyle, J., 1995. Na-Cl-Br systematics of mineralizing brines in Mississippi Valley–type deposits. Geology 23, 641–644.
Kenderes, S.M., Appold, M.S., 2017. Fluorine concentrations of ore fluids in the Illinois-Kentucky district: Evidence from SEM-EDS analysis of fluid inclusion decrepitates. Geochimica et Cosmochimica Acta 210, 132–151.
Kiyosu, Y., Krouse, H.R., 1989. Carbon isotope effect during abiogenic oxidation of methane. Earth and Planetary Sciences Letter 95, 302–306.
Kiyosu, Y., Krouse, H.R., 1990. The role of organic-acid in the abiogenic reduction of sulfate and the sulfur isotope effect. Geochemical Journal 24, 21–27.
Kiyosu, Y., Imaizumi, S., 1996. Carbon and hydrogen isotope fractionation during oxidation of methane by metal oxides at temperatures from 400 degrees to 530 degrees C. Chemical Geology 133, 79–287.
Krouse, H.R., Viau, C.A., Eliuk, L.S., Ueda, A., Halas, S., 1988. Chemical and isotopic evidence of thermochemical sulphate reduction by light hydrocarbon gases in deep carbonate reservoirs. Nature 333, 415–419.
Lambert, J.M., Simkovich, G., Walker, P.L., 1998. The kinetics and mechanism of the pyrite-to-pyrrhotite transformation. Metallurgical and materials transactions B 29, 385–396.
Leach, D.L., Bradley, D., Lewchuk, M.T., Symons, D.T., de Marsily, G., Brannon, J., 2001. Mississippi Valley-type lead–zinc deposits through geological time: implications from recent age-dating research. Mineralium Deposita 36, 711–740.
Lu, H., Chen, T.S., Liu, J.Z., Peng, P.A., Lu, Z.H., Ma, Q.L., 2010. Yields of H_2S and gaseous hydrocarbons in gold tube experiments simulating thermochemical sulfate reduction reactions between $MgSO_4$ and petroleum fractions. Organic Geochemistry 41, 1189–1197.
Lu, H., Greenwood, P., Chen, T., Liu, J., Peng, P.A., 2011. The role of metal sulfates in thermochemical sulfate reduction (TSR) of hydrocarbons: Insight from the yields and stable carbon isotopes of gas products. Organic Geochemistry 42, 700–706.
Lu, H., Greenwood, P., Chen, T., Liu, J., Peng, P.A., 2012. The separate production of H_2S from the thermal reaction of hydrocarbons with magnesium sulfate and sulfur: Implications for thermal sulfate reduction. Applied Geochemistry 27, 96–105.
Lu, H., Shi, Q., Lu, J., Sheng, G.Y., Peng, P.A., Hsu, C.S., 2013. Petroleum sulfur biomarkers analyzed by comprehensive two-dimensional gas chromatography sulfur-specific detection and mass spectrometry. Energy & Fuels 27, 7245–7551.
Machel, H.G., Krouse, H.R., Sassen, R., 1995. Products and distinguishing criteria of bacterial and thermochemical sulfate reduction. Applied Geochemistry 10, 373–389.
Machel, H.G., 2001. Bacterial and thermochemical sulfate reduction in diagenetic settings—old and new insights. Sedimentary Geology 140, 143–175.
Manzano, B.K., Fowler, M.G., Machel, H.G., 1997. The influence of thermochemical sulphate reduction on hydrocarbon composition in Nisku reservoirs. Brazeau river area, Alberta, Organic Geochemistry 27, 507–521.
Ma, Q.S., Ellis, G.S., Amrani, A., Zhang, T.W., Tang, Y.C., 2008. Theoretical study on the reactivity of sulfate species with hydrocarbons. Geochimica et Cosmochimica Acta 72, 4565–4576.
Tauson, V.L., Sapozhnikov, A.N., uson and Sapozhnikov (2005). Stability of the modulated structure of Baikal lazurite and its recrystallization at a temperature of 600°C over a wide range of sulfur dioxide fugacities. Crystallogrraphy Reports 50, S1–S9.
Nakai, S., Halliday, A.N., Kesler, S.E., Jones, H.D., 1990. Rb–Sr dating of sphalerites from Tennessee and the genesis of Mississippi Valley type ore deposits. Nature 346, 354.
Navarro-Ciurana, D., Cardellach, E., Vindel, E., Griera, A., Gómez-Gras, D., Corbella, M., 2017. Sulfur and lead isotope systematics: Implications for the genesis of the Riópar Zn-(Fe-Pb) carbonate-hosted deposit (Prebetic Zone, SE Spain). Ore Geology Reviews 91, 928–944.
Orr, W.L., 1977. Geologic and geochemical controls on the distribution of hydrogen sulfide in natural gas. In: Campo, R., Goni, J. (Eds.), Advances in Organic Geochemistry. Enadimsa, Madrid, pp. 572–597.
Orr, W.L., Sinninghe Damsté, J.S., 1990. Geochemistry of sulfur in petroleum systems. Geochemistry of Sulfur in Fossil Fuels, 2–29.
Pan, C.C., Yu, L.P., Liu, J.Z., 2006. Chemical and carbon isotopic fractionations of gaseous hydrocarbons during abiogenic oxidation. Earth and Planetary Science Letters 246, 70–89.
Pelovski, Y., Petkova, V., Nikolov, S., 1996. Study of the mechanism of the thermochemical decomposition of ferrous sulphate monohydrate. Thermochimica Acta 274, 273–280.
Perkins, R.B., Gray, Z.N., Grathoff, G., Hugo, R., 2016. Characterization of natural and synthetic floating iron surface films and their associated waters. Chemical Geology 444, 16–26.
Powell, T.G., Macqueen, R.W., 1984. Precipitation of sulfide ores and organic matter—sulfate reduction at Pine Point, Canada. Science 224, 63–66.
Rickard, D., 1997. Kinetics of pyrite formation by the H_2S oxidation of iron (II) monosulfide in aqueous solutions between 25 and 125 °C: The rate equation. Geochimica et Cosmochimica Acta 61, 115–134.
Schmid, J.C., Connan, J., Albrecht, P., 1987. Occurrence and geochemical significance of long-chain dialkylthiacyclopentanes. Nature 329, 54–56.
Schoonen, M.A.A., Barnes, H.L., 1991. Reactions forming pyrite and marcasite from solution: II. Via FeS precursors below 100 °C. Geochimica et Cosmochimica Acta 55, 1505–1514.
Seewald, J.S., 2003. Organic–inorganic interactions in petroleum-producing sedimentary basins. Nature 426, 327.
Sośnicka, M., Lüders, V., 2019. Super-deep, TSR-controlled Phanerozoic MVT type Zn-Pb deposits hosted by Zechstein-2 gas reservoir carbonate (Ca2), Lower Saxony Basin, Germany. Chemical Geology 508, 62–77.
Spangenberg, J.E., Fontbote, L., Macko, S.A., 1999. An evaluation of the inorganic and organic geochemistry of the San Vicente mississippi valley-type zinc-lead district, central Peru; implications for ore fluid composition, mixing processes, and sulfate reduction. Economic Geology 94, 1067–1092.
Stoler A., Spiro B., Amrani A., Aizenshtat Z., Evaluation of $\delta^{34}S$ changes during stepwise pyrolysis of bituminous rocks and type II-S kerogen, 21st IMOG meeting, Krakow, Poland, Organic Geochemistry., 2003 103–104.
Sverjensky, D.A., 1986. Genesis of Mississippi Valley-type lead-zinc desposits. Annual Review of Earth and Planetary Sciences 14, 177–199.
Tang, Y., Ellis, G.S., Zhang, T., Jin, Y., 2005. Effect of aqueous chemistry on the thermal stability of hydrocarbons in petroleum reservoirs. Geochimica et Cosmochimica Acta Supplement 69, A559.
Thom, J., Anderson, G.M., 2008. The role of thermochemical sulfate reduction in the origin of Mississippi Valley-type deposits. I. Experimental results. Geofluids 8, 16–26.
Toland, W.G., 1960. Oxidation of organic compounds with aqueous sulphate. Journal of American Chemistry Society 82, 1911–1916.
Truche, L., Berger, G., Destrigneville, C., Pages, A., Guillaume, D., Giffaut, E., Jacquot, E., 2009. Experimental reduction of aqueous sulphate by hydrogen under hydrothermal conditions: Implication for the nuclear waste storage. Geochimica et Cosmochimica Acta 73, 4824–4835.
Truche, L., Bazarkina, E.F., Barré, G., Thomassot, E., Berger, G., Dubessy, J., Robert, P., 2014. The role of S_3^- ion in thermochemical sulphate reduction: Geological and geochemical implications. Earth and Planetary Science Letters 396, 190–200.
Wang, Q., Lu, H., Shen, C., Liu, J., Peng, P.A., Hsu, C.S., 2014. Impact of inorganically bound sulfur on late shale gas generation. Energy & Fuels 28, 785–793.
Wei, Y., Han, B., Hu, X., Lin, Y., Wang, X., Deng, X., 2012. Synthesis of Fe_3O_4 nanoparticles and their magnetic properties. Procedia Engineering 27, 632–637.
White, D.E., 1968. Environments of generation of some base-metal ore deposits. Economic Geology 63, 301–335.
Wiltowski, T., Hinckley, C.C., Smith, G.V., Nishizawa, T., Saporoschenko, M., Shiley, R. H., Webster, J.R., 1987. Kinetics and mechanisms of iron sulfide reductions in hydrogen and in carbon monoxide. Journal of Solid State Chemistry 71, 95–102.
Worden, R.H., Smalley, P.C., 1996. H_2S-producing reactions in deep carbonate gas reservoirs: Khuff formation, Abu Dhabi. Chemical Geology 133, 157–171.
Worden, R.H., Smalley, P.C., Cross, M.M., 2000. The influence of rock fabric and mineralogy on thermochemical sulfate reduction: Khuff formation, Abu Dhabi. Journal of Sedimentary Research 70, 1210–1221.
Worden, R.H., Smalley, P.C., 2004. Does methane react during thermochemical sulfate reduction? Proof from the Khuff Formation, Abu Dhabu. In: Wanty, R., Seal, R.R. (Eds.), Water Rock Interaction 2004. Taylor and Francis Group, London, pp. 1049–1053.
Zboril, R., Mashlan, M., Petridis, D., Krausova, D., Pikal, P., 2002. The role of intermediates in the process of red ferric pigment manufacture from $FeSO_4.7H_2O$. Hyperfine Interactions 139 (140), 437–445.
Zhang, T., Ellis, G.S., Wang, K.S., Walters, C.C., Kelemen, S.R., Gillaizeau, B., Tang, Y., 2007. Effect of hydrocarbon type on thermochemical sulfate reduction. Organic Geochemistry 38, 897–910.
Zhang, T., Amrani, A., Ellis, G.S., Ma, Q., Tang, Y., 2008a. Experimental investigation on thermochemical sulfate reduction by H_2S initiation. Geochimica et Cosmochimica Acta 72, 3518–3530.
Zhang, T., Ellis, G.S., Walters, C.C., Kelemen, S.R., Wang, K.S., Tang, Y., 2008b. Geochemical signatures of thermochemical sulfate reduction in controlled hydrous pyrolysis experiments. Organic Geochemistry 39, 308–328.
Zhang, T., Ellis, G.S., Ma, Q., Amrani, A., Tang, Y., 2012. Kinetics of uncatalyzed thermochemical sulfate reduction by sulfur-free paraffin. Geochimica et Cosmochimica Acta 96, 1–17.